FDTD SIMULATIONS OF RECONFIGURABLE ELECTROMAGNETIC BAND GAP STRUCTURES FOR MILLIMETER WAVE APPLICATIONS

R. W. Ziolkowski

Department of Electrical & Computer Engineering
The University of Arizona
1230 E. Speedway Blvd.
Tucson, AZ 85721-0104, USA

Abstract—Metallo-dielectric electromagnetic bandgap (EBG) structures are studied in the millimeter regime with a finite difference time domain (FDTD) simulator. Several EBG waveguiding structures are considered for millimeter-wave power splitting, switching and filtering operations. It is demonstrated that triangular EBG structures lend themselves naturally to the design of Y-power splitters. Square EBG structures with circular and square rods are shown to lead naturally to straight in-line waveguide filter applications. Comparisons between EBG millimeter-wave waveguide filters formed with dielectric and metallic rods are given. It is shown that high quality broad bandwidth, millimeter-wave bandstop filters can be realized with square EBG structures with circular metallic rods. It is demonstrated that multiple bandstop performance in a single device can be obtained by cascading together multiple EBG millimeter-wave waveguide filters. It is also demonstrated that one can control the electromagnetic power flow in these millimeter-wave EBG waveguide devices by introducing additional local defects. It is shown that the Y-power splitter can be made reconfigurable by using imposed current distributions to achieve these local defects and, consequently, that a millimeter-wave EBG switch can be realized.

1 **Introduction**

2 **FDTD Simulator**

3 **Simulation Result**

1. INTRODUCTION

Since the recent rediscovery of their usefulness in the optics area, finite periodic structures that exhibit band gap effects have led to an explosion of activity throughout the frequency spectrum. The so-called photonic band gap (PBG) structure has become a very important subject in the optics regime. For instance, nanometer and micron sized PBG devices are currently being explored to enhance the performance of microcavity laser mirrors and for their applications in a variety of optical systems associated with communications, data storage, and computing [1–11]. In the microwave area numerous research groups are using microwave band gap (MBG) structures, for example, to modify the frequency performance of microstrip lines, to suppress surface wave modes associated with microstrip fed patch antennas and to enhance the radiation characteristics of a variety of wire antennas [12–25]. In particular, they have also been used recently to achieve reconfigurable, planar cavity resonators and filters [26, 27].

To achieve a more consistent terminology and to address the concerns of microwave engineers that the descriptor "PBG" is inappropriate for microwave devices and their applications, a structure that produces an absence of a response in either frequency or wavenumber (band gap) for some polarization or angle of incidence or vector orientation (electromagnetic properties) will be denoted here as an electromagnetic band gap (EBG) structure. This terminology encompasses the frequency regimes from quasi-statics to light and beyond.

A number of metallo-dielectric EBG structures have been studied extensively [28–39]. They have been shown to have several important properties that could be exploited in the optical regime for a variety of applications. What is shared in common between these structures is the presence of one material type that is highly dispersive and leads to a large negative permittivity in the frequency region of interest, hence, high reflectivity there. This is particularly true at optical frequencies where dispersive effects occur even for copper, silver, or gold conductors. This is due to the fact that at such high frequencies, the imaginary part of the index of refraction can

be larger than its real part. Lorentz or Drude (Lorentz model with zero resonance frequency) material models for the metal are needed rather than a simple conductivity model. These frequency dependent material models have been included readily in FDTD simulators for these EBG applications. The ability of the FDTD approach (see [40–41] for extensive reviews on this approach and its applications) to model dispersive materials has been demonstrated by several research groups. For example, our FDTD simulator also has been used recently to study material dispersive effects in EBG structures [42]. This allowed the study of metallo-dielectric EBG structures in the optics regime; e.g., layered structures formed from alternating layers of dielectrics and metals excited at optical frequencies. Note, however, that at millimeter wavelengths the simple, frequency independent bulk conductivity model is still generally an adequate description of a metal such as copper. This greatly simplifies the millimeter wave simulations to be considered here.

The FDTD approach has several advantages for modeling EBG structures. It can readily incorporate a variety of complex materials. It can deal with the very complex geometries associated with EBG structures themselves and their integration with other devices. It can handle either single cycle and multi-cycle excitations; this allows investigations of the broad and narrow bandwidth responses of an EBG structure from a single simulation environment. For example, our 3D-FDTD simulator has been used to model an EBG structure that achieved an electronically controlled, reconfigurable EBG filter [43].

It has also been demonstrated that EBG structures can be used across the frequency spectrum to form extremely narrow bandwidth filters and extremely small waveguiding structures and devices [1, 44–57]. Waveguide channels in a regular EBG structure are formed by the removal of particular sets of objects from which it is constructed. For instance, for optical communication applications a typical wavelength is $1.5\,\mu$m in silicon, $\lambda_{Si} = \lambda/n_{Si} \sim 430\,$nm. If an EBG structure consisted of a square lattice of vertical, circular air holes in a horizontal Si slab, an optical waveguide can be formed in the slab by refilling, for example, one column of the air holes. The remaining air holes act to form the walls of the waveguide. Fundamental mode operation in such a EBG waveguide can be achieved if the separation between the air holes surrounding the refilled column is slightly larger than $\lambda_{Si}/2 = 215\,$nm. The use of these defect EBG structures as nanometer waveguiding environments may provide a means to achieve photonic nano-circuits.

Because of the wavelength scaling of EBG structures, they also

have significant potential for important applications in the millimeter-wave regime. This paper investigates the use of the FDTD approach to model the behavior of EBG waveguiding structures for millimeter wave power splitting, switching and filtering operations. The emphasis on the millimeter wave applications is encouraged by the acknowledgment that many filtering operations in the microwave integrated circuit (MIC) regime, say in the X-band region, can be achieved with other well-known planar structures, e.g., stub tuners. However, because the structure sizes decrease as the frequency proceeds into the millimeter wave regime, e.g., at $300\,\text{GHz}$ a $\lambda/4$ stub is $250\,\mu\text{m}$ long, and, thus, fabrication tolerances become more stringent, alternative approaches to achieve devices for millimeter wave integrated circuit (MMIC) applications need to be explored. The FDTD simulator used in the present EBG waveguide analysis has been validated previously with modeling of those optical waveguiding structures and devices [54–57]. Those studies dealt with basic optical sub-wavelength waveguiding structures in square and triangular EBG structures formed in a dielectric substrate with air holes or metallic rods and fed by dielectric waveguides, as well as free-space beams scattering from EBG structures formed from a set of dielectric or metallic rods. The triangular EBG structures lend themselves to the design of Y-power splitters. Square EBG structures with circular and square rods naturally lead to straight waveguide filter applications or to waveguides with right angle bends. By introducing further defects into the EBG structures, we have demonstrated that control of the electromagnetic power flow in these EBG waveguides can be achieved and that with such additional defects, defect-based resonators, filters, and switches can be realized, as has been demonstrated experimentally at microwave frequencies [26, 27, 43].

Emphasis will be given to metallo-dielectric EBG structures and all EBG structures will be characterized with our FDTD simulator. Dielectric waveguides are commonly found in millimeter wave applications. Only Gallium Arsenide (GaAs) substrates will be considered here. The integration of copper-based EBG structures with these dielectric waveguides leads to several interesting devices that are efficient and small in size. It will be demonstrated that triangular EBG structures lend themselves to the design of millimeter wave Y-power splitters. Moreover, it will be shown how reconfigurability of the Y-power splitter can be achieved by using imposed current distributions and, consequently, how a millimeter-wave EBG switch can be realized. A basic in-line waveguide filter will be designed with EBG structures with circular rods. Results will be presented to illustrate that a broad bandwidth, millimeter wave bandstop filter can be achieved. By
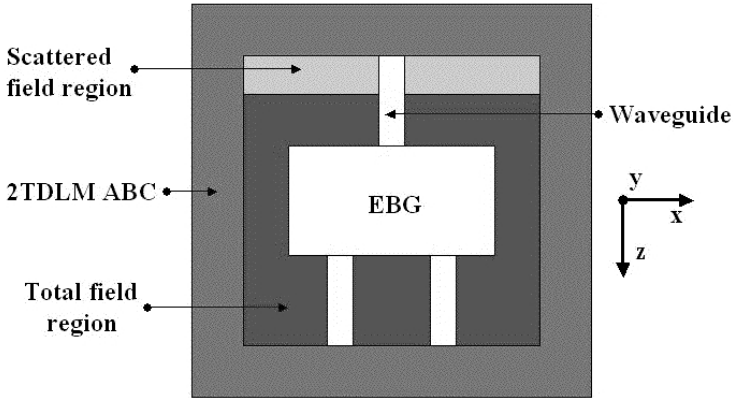
Figure 1. FDTD Simulation Space.

varying the EBG structure, the center frequency of the filter can be changed. Thus, by cascading multiple EBG structure filters, multiple bandstop performance can be realized in a single device. Contrasts between filters realized with square EBG structures with square metal rods and circular and square air holes will be given.

2. FDTD SIMULATOR

The millimeter wave configurations that were investigated consist of an EBG structure formed in a dielectric block by embedding metallic (and dielectric) posts within it. The EBG structure is fed with one dielectric waveguide. In the case of the Y-power splitter, it has two output ports, each consisting of a single dielectric waveguide of the same type. The basic FDTD simulation region corresponding to this case is shown in Fig. 1. In the in-line filter case, only a single output dielectric waveguide of the same type is present and is an extension of the input waveguide.

Note that only semi-infinite (2D) EBG structures were considered for this study. The slab waveguides and the rods (holes) were oriented with their infinite dimension along the y-axis. The FDTD simulations were then restricted to the TE case (E_y, H_x, and H_z field components) since this field configuration allows the EBG structure to have its largest effect when the rods are metal, i.e., the electric field on the high conductivity cylinders becomes extremely small, $E_y = E_{\tan} \sim 0$. They will thus force a large perturbation in the electric field distribution within the dielectric block. Only square cells of sidelength Δ were used

in the FDTD lattice. The z-axis was taken to be along the length of the waveguide; the x-axis was taken to be along the transverse dimension of the waveguide.

In all of the cases reported below, the background medium was free space. The dielectric material was selected to be GaAs. The material constants are $\epsilon = 13.0032\epsilon_0$, $\mu = \mu_0$, $\sigma = 0.0$ [58]. The waveguides were taken to be 20 FDTD cells wide unless otherwise noted. The center frequency for all the simulations was set at $f_0 = 100\,\text{GHz}$, which corresponds to a free space wavelength $\lambda_0 = 3.0\,\text{mm}$. The wavelength in the waveguide is thus $\lambda_g = \lambda_0/\sqrt{13.0032} = 832\,\mu\text{m}$. The cell size was set at $\Delta = \lambda_0/115$ in all of the cases reported below. It was found that with this choice the resulting waveguide width $d = 0.627\lambda_g$ produced desired results nearly centered about f_0. Moreover, this discretization value produces very accurate simulation results. This waveguide width is slightly larger than half of the center wavelength in the dielectric; hence, there should be only the fundamental symmetric mode present in the EBG waveguide. The metal rods were taken to be copper, which has the material properties $\epsilon = \epsilon_0 + i\sigma/\omega$, where $\sigma = 5.8 \times 10^7\,\text{S/m}$, and $\mu = \mu_0$. Thus, the loss tangent in the metal rods was $\sigma/(\omega\epsilon_0) = 8.02 \times 10^5$; hence, they were treated as metals obeying Ohm's Law, i.e., a simple conductivity model was used. Some comparisons of cases using dielectric rather than metallic rods will be mentioned below; in these cases, the rods were air-filled holes. Any rods that are removed from the EBG lattice to form the defect waveguides are re-filled with the GaAs substrate.

The incident waveguide field is launched from a total field/scattered field boundary [40]. It is defined by the product of spatial and temporal distributions. The initial spatial distribution is defined by the lowest order, dominant symmetric mode for the dielectric slab waveguide corresponding to the input waveguide. To produce this mode, one is required ([59], 159–164) to solve the guidance condition (transcendental) equation for the transverse wavenumber, k_x, in the waveguide.

$$\left[\omega^2(\epsilon\mu - \epsilon_0\mu_0) - k_x^2\right]d = \frac{\mu_0}{\mu}(k_x d)\tan\left(\frac{k_x d}{2}\right) \qquad (1)$$

A simple root solving program was written in order to find k_x whenever the waveguide configuration changed.

The time history of the driving field at the total-field/scattered-

field plane was chosen to be the multiple cycle $m - n - m$ pulse:

$$
f(t) = \begin{cases}
g_{\text{on}}(t)\sin(\omega_0 t) & \text{for } 0 \leq t < mT_p \\
\sin(\omega t) & \text{for } mT_p \leq t \leq (m+n)T_p \\
g_{\text{off}}(t)\sin(\omega_0 t) & \text{for } (m+n)T_p < t \leq (m+n+m)T_p \\
0 & \text{for } t > (m+n+m)T_p
\end{cases} \tag{2}
$$

where $T_p = 2\pi/\omega_0 = 1/f_0$ is the period of one cycle and the three-derivative smooth window functions

$$
g_{\text{on}}(t) = 10.0x_{\text{on}}^3 - 15.0x_{\text{on}}^4 + 6.0x_{\text{on}}^5
$$

$$
g_{\text{off}}(t) = 1.0 - [10.0x_{\text{off}}^3 - 15.0x_{\text{off}}^4 + 6.0x_{\text{off}}^5] \tag{3}
$$

where $x_{\text{on}} = 1.0 - (mT_p - t)/mT_p$ and $x_{\text{off}} = [t - (m+n)T_p]/mT_p$. The $m - n - m$ pulse is a sinusoidal signal that has a smooth windowed turn-on for m cycles, a constant amplitude for n-cycles, and then a smooth windowed turn-off for m-cycles; hence, it has an adjustable bandwidth (through the total number of cycles $m + n + m$) centered at the frequency f_0. For all of the cases considered below, both the broad bandwidth 3-cycle, $1 - 1 - 1$ pulse and the narrow bandwidth 200-cycle, $5 - 190 - 5$ pulse were used to probe the EBG structures.

The simulation region is terminated with the two dimensional version of the lossy 2TDLM ABC (absorbing boundary condition) [60–62]. This form of the ABC allows one to extend the input and output dielectric waveguides completely into the ABC regions. The 2TDLM ABC layers were taken to be 10 cells thick with a quadratic spatial variation; they were optimized by running several waveguide only cases (pick a value for the maximum loss parameter in the layers, launch the pulse into the waveguide, let the pulse propagate along the waveguide and interact with the ABC layers, and then measure the size of the reflected pulse). For the 3 cycle pulse cases, reflections smaller than $-75\,\text{dB}$ were achieved over the frequency band of interest.

The EBG structure consisted of either the triangular (2a) or the square lattice (2b) configurations shown in Fig. 2. The triangular lattice EBG structures under consideration consisted of 13 columns $\times$ 30 rows of circular copper cylinders embedded in the GaAs block. The radius of each cylinder was $r = 5.0\Delta$; the horizontal distance between the centers of the cylinders was offset $= 15.0\Delta$; and the vertical distance between the centers of the cylinders was $a/2 = 9.0\Delta$. The size of the entire Y-power splitter device was 14 offset $\times 16a = 210\Delta \times 288\Delta = 1.826\lambda_0 \times 2.504\lambda_0 = 41.15\,\text{mm}^2$. The waveguides within the EBG structure were formed by removing a particular set of cylinders. Again, the waveguide width was 20 cells, i.e., $2(\text{offset} - r) = 20\Delta$. The
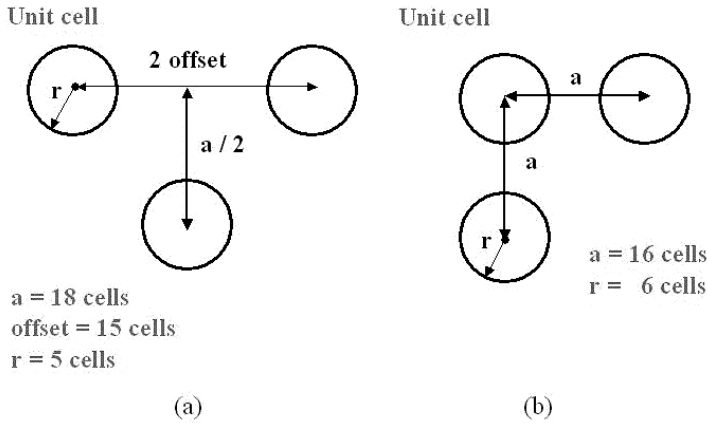
Figure 2. EBG triangular (a) and square (b) lattice configuration.

total problem size was 538 cells long in z and 340 cells wide in x. These simulations were run with Δt at 1.0 times the Courant limit for 10,000 time steps. The square lattice EBG structures under consideration below for the in-line filters consisted of 11 columns $\times$ 30 rows of circular (and square) copper cylinders embedded in the GaAs block. The distance between the centers of each rod was $a = 16.0\Delta$; each circular rod has a radius $r = 6.0\Delta$. The size of the entire in-line filter was $14a \times 31a = 224\Delta \times 496\Delta = 1.948\lambda_0 \times 4.313\lambda_0 = 75.62\,\text{mm}^2$. The corresponding square rods had a sidelength of $2r$. The total problem size was 850 cells long in z and 320 cells wide in x. These simulations were run with Δt at 1.0 times the Courant limit for 10,000 time steps.

The electromagnetic behavior of the various EBG structures were characterized by various power transmission and reflection coefficients. They were obtained by measuring the electric and magnetic fields at all of the points on specified surfaces in the FDTD mesh, fast Fourier transforming each of these time histories, forming the time-averaged Poynting's vector components associated with each point on this surface, and then forming the total time-averaged Poynting's vector through those surfaces by summing over all of the points on that surface the time-averaged Poynting's vector flux values associated with each point. In all the cases discussed below, the total power was obtained across the input waveguide 10 cells from the total field/scattered field plane into the scattered field region (reflected power spectrum), across the input waveguide $2a$ before the EBG structure (input power

spectrum) and across each of the output waveguides $2a$ after the EBG structure (transmitted power spectrum). Thus, with one broad bandwidth pulse simulation the frequency domain transfer function of the finite EBG structure was generated. When desired, the optimal operating frequency was determined and the corresponding narrow bandwidth excitation cases were run to characterize the performance of the device at a selected frequency.

3. SIMULATION RESULT

Using the FDTD simulator, results were obtained for the Y-power splitter with no defect, for the Y-power splitter with an additional defect to cause a switch in the flow of power, and for the in-line filter. These results are presented below. It is demonstrated that the triangular EBG structures provides the construction of an effective power splitter; that a single defect can effectively switch the power flow from both arms into one arm of the Y-power splitter; and that the square EBG structure provides the construction of an effective, in-line broad stopband filter.

3.1. Y-Power Splitter Results

The two-dimensional triangular EBG FDTD configuration shown in Fig. 3 (and defined explicitly in Fig. 2a) was considered. In this figure the shaded regions are GaAs (the waveguides and the EBG background substrate) and the black regions are the locations of the metallic rods. The 3-cycle broad bandwidth input pulse results are summarized in Fig. 4.

The normalized spectra of the input waveguide pulse, the reflected waveguide pulse and the waveguide pulse exiting the power splitter through the right arm (the left arm values are the same) are presented. They have been normalized by the peak of the power spectrum of the input waveguide pulse. Several noticeable aspects of the data deserve comment.

The fact that there are peaks in the reflected power spectrum which exceed at a few frequencies the input power is explained as follows. The input power represents the power measured only within the input dielectric waveguide. It does not take into account the input power that exists outside of the waveguide. The reflected and transmitted powers are also measured, respectively, only within the input and the output wave guides. However, with the reflected power sampling surface being within the near field of the entire EBG structure, the power scattered from the entire EBG structure will also
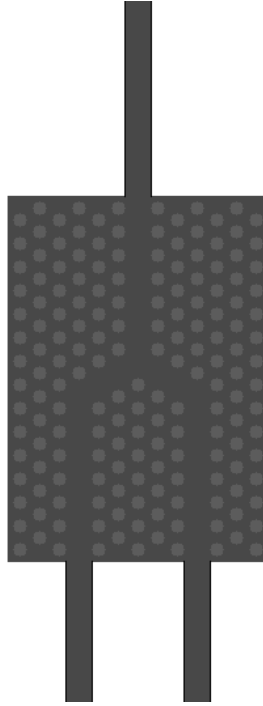
Figure 3. EBG triangular lattice Y-power splitter with no defect geometry.
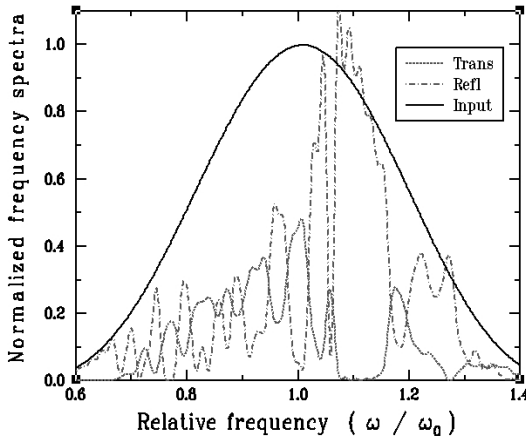

Figure 4. Normalized power spectra results for a broad bandwidth excitation of the EBG triangular lattice Y-power splitter with no defect.

be collected there. When the reflectivity within the waveguide is close to one, this additional power can cause these anomalous features. One way to avoid this situation would be to extend the simulation region away from the EBG structure and measure the reflected field in the waveguide much farther away from it. This does significantly increase the computational costs of the simulations. Another issue is the the short pulse, hence broad bandwidth, nature of the excitation. There is no convenient way to time-gate the data to avoid these unwanted contributions. The reflected power has contributions from the reflections occurring at the input port, the Y-junction, and from the output ports (no transmitted power), as well as power re-radiated from the entire EBG structure. These power contributions all arrive at the measurement port at different times. Finally, numerical noise will corrupt the data some. Note that these anomalous features commonly appear in the Fourier transform data when there is negligible output power; they do not appear in the time histories of the fields. This behavior is again apparent in the total power summations. For instance, there is a peak in the transmitted power and a null in the reflected power near the center frequency of the input power at $f/f_0 = 1.0051$ as expected. However, the total reflected power is 3.85% of the input power; the total power output from the device is $2 \times 48.41\% = 96.82\%$ of the input power. Knowing that some small amount of power resides in the EBG structure or has been radiated from it, this about 0.67% too much power, at least. Nonetheless, these values are within the numerical noise and they are reasonably good approximations of those found below with the narrow bandwidth excitation.

Notice, however, that the suspect reflected and transmitted power features also indicate that significant broad bandwidth stopband filtering can be achieved with such a triangular EBG structure. This observation actually encouraged the in-line filter investigations summarized below.

Using $f = f_0$ as the center frequency of the input signal for the narrow bandwidth excitation, the EBG structure's performance was characterized. The electric field intensity in the simulation space, once steady state operation is achieved, is shown in Fig. 5. Note that the location of the total field/scattered field source plane is apparent in this figure about one-third of the way down from the end of the input waveguide. The impact of the interfaces between the input dielectric waveguide and the dielectric boundaries of the EBG region, and the two output dielectric waveguides and that EBG region, can also be ascertained from this figure.

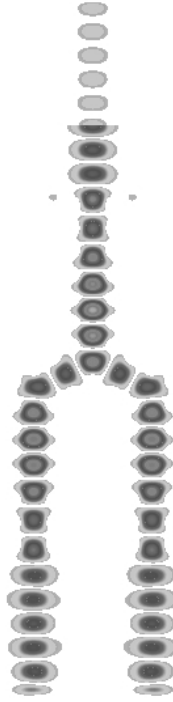The measured time histories were appropriately truncated to

Figure 5. Electric field intensity distribution for a narrow bandwidth excitation in the EBG triangular lattice Y-power splitter with no defect.

account for the time of arrivals of the fields at the reflected and transmitted field collection ports. The resulting steady state spectra of the input waveguide pulse, the reflected waveguide pulse and the waveguide pulse exiting the power splitter through the right arm (the left arm values are the same) are presented in Fig. 6. They have been normalized by the peak of the power spectrum of the input waveguide pulse. The total reflected power is 4.22% of the input power; the total power output from the device is $2 \times 47.78\% = 95.56\%$ of the input power. Thus at the center frequency, about 0.22% of the input power is stored in the EBG structure or radiated into free space. These values correspond to an $S_{11} = -27.50\,\text{dB}$ and an insertion loss of $-0.39\,\text{dB}$; they indicate that this EBG-based Y-power splitter could be a very efficient millimeter-wave device.
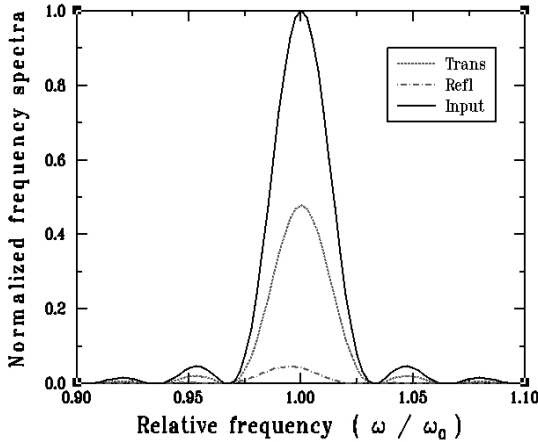
Figure 6. Normalized power spectra results for a narrow bandwidth excitation of the EBG triangular lattice Y-power splitter with no defect.

3.2. Y-Power Splitter Switch Results

By introducing an additional post into the triangular EBG configuration, as shown in Fig. 7, one can force the flow of electromagnetic power into the right arm. In this figure the shaded regions are again GaAs (the waveguides and the EBG background substrate) and the black regions are the locations of the metallic rods. Note again that the location of the total field/scattered field source plane is apparent in this figure about one-third of the way down from the end of the input waveguide. The location of the additional control defect rod is also apparent. The impact of the interfaces between the input dielectric waveguide and the dielectric boundaries of the EBG region, and the two output dielectric waveguides and that EBG region, can again be ascertained from this figure.

This control defect configuration was tested with the narrow bandwidth excitation centered at f_0. The electric field intensity in the simulation space once steady state operation is achieved is shown in Fig. 8. The measured time histories were appropriately truncated to account for the time of arrivals of the fields at the reflected and transmitted field collection ports. The resulting steady state spectra of the input waveguide pulse, the reflected waveguide pulse and the waveguide pulse exiting the power splitter through the right arm (the left arm values are the same) are presented in Fig. 9. They have been normalized by the peak of the power spectrum of the input waveguide
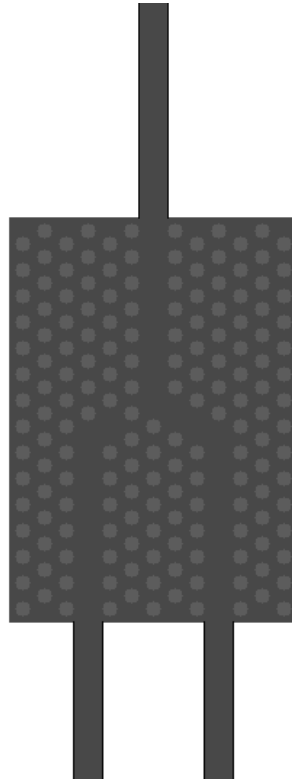
Figure 7. EBG triangular lattice Y-power splitter with one defect geometry.

pulse. The total reflected power is 14.98% of the input power; the total power output from the device is 84.90% of the input power. Thus at the center frequency, about 0.12% of the input power is now stored in the EBG structure or radiated into free space. These values correspond to an $S_{11} = -16.49\,\mathrm{dB}$ and an insertion loss of $-1.42\,\mathrm{dB}$. Clearly, the additional post does switch a majority of the power from the left arm into the right arm. It also increases the amount of reflected power. The smallness of the waveguiding environment coupled with the abrupt change at the junction produces this larger reflected power value.

It must be emphasized that this configuration could be used as a switch to control the flow of electromagnetic power in a MMIC application. How could one achieve the presence of an additional metallic rod in the dielectric block? The following solution is proposed.

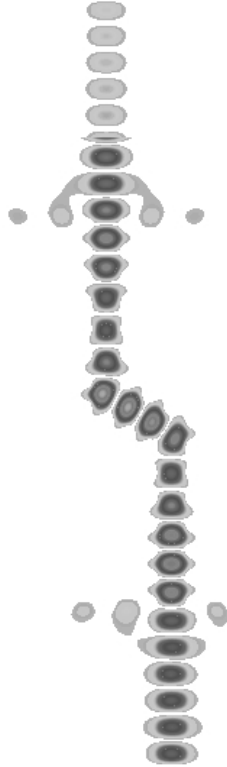Consider introducing a steady state current filament into the

Figure 8. Electric field intensity distribution for a narrow bandwidth excitation in the EBG triangular lattice Y-power splitter with one defect.

dielectric substrate. The presence of the electrons in this current filament cause a modification of the permittivity. If the number of electrons per unit volume is N_e and the corresponding plasma frequency is $\omega_p^2 = N_e e^2/(\epsilon_0 m_e)$, the effective permittivity would become ([59], pp. 46)

$$\epsilon_{\text{eff}} = \epsilon - \frac{N_e e^2}{m_e \omega^2} = \epsilon \left(1 - \frac{\epsilon_0}{\epsilon} \frac{\omega_p^2}{\omega^2} \right) \tag{4}$$

Consequently, if ω_p were large enough so that $f_p \gg f = 100\,\text{GHz}$, i.e., if enough electrons were present, then $\epsilon_{\text{eff}} < 0$ and the current filament would become reflective at the desired operating frequency.

To maintain the EBG and additional defect geometry, one could consider replacing the defect rod with a current filament of the same
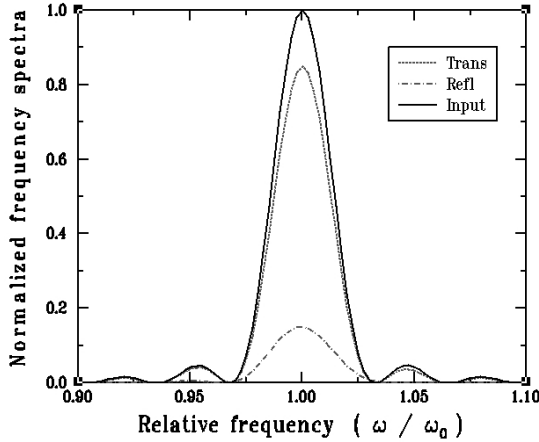
Figure 9. Normalized power spectra results for a narrow bandwidth excitation of the EBG triangular lattice Y-power splitter with one defect.

radius, $r = 5$ cells, as the metallic rod it is supposed to mimic. A practical realization of the 2D EBG structure occurs if the height of the GaAs slab were restricted to a sub-wavelength size (total internal reflection would then provide the waveguiding effect in this third dimension and no higher order modes would be allowed). Thus, let this height $h = \lambda_0/(2.77\sqrt{\epsilon}) = 300\,\mu$m and assume a 1 V potential is applied across the height of the slab. Since the resistivity of undoped GaAs is $\rho = 3.7 \times 10^6$ ohm-m [63], the resulting current would be

$$
\begin{aligned}
I &= \frac{V}{R} = \frac{VA}{h\rho} = \frac{V\pi r^2}{h\rho} \\
&= \frac{(1\text{V})(3.14 \times (5 \times 0.003 \text{ m}/115)^2)}{(0.0003 \text{ m}) \times (3.7 \times 10^6 \text{ohm-m})} \\
&= 4.815 \times 10^{-11} \text{Amps}
\end{aligned}
\tag{5}
$$

This current corresponds to $4.815 \times 10^{-11}/1.6 \times 10^{-19} = 3.00 \times 10^8$ electrons per second flowing into the substrate. The corresponding electron number density per second would thus be $N_e = 3.00 \times 10^8/Ah = 1.871 \times 10^{19}$ m^{-3}; and, hence, the plasma frequency would be $\omega_p = 5.64 \times 10^4\sqrt{N_e} = 2.44 \times 10^{14}$ Hz $= 3.88 \times 10^2\omega_0$. The corresponding amplitude reflection coefficient would be

$$R = \frac{1 - \sqrt{\epsilon/\epsilon_0}}{1 + \sqrt{\epsilon/\epsilon_0}} = \frac{1 - 387.98j}{1 + 387.98j} \approx -1.00 \qquad (6)$$

Thus the current filament would indeed look like a metallic object to waves whose frequency is f_0. This result then implies that by reconfiguring the Y-power splitter with a "current post", an effective millimeter-wave switch could be realized.

Note that this result also implies that with two current elements, one for each output waveguide mouth, an effective device could be achieved that could mimic the function of a circulator without the presence of a magnetic material. Moreover, this current filament result implies, in principle, that the entire EBG structure could be constructed from an array of current filaments. This concept leads to the possibility of an entirely reconfigurable EBG structure in the millimeter wavelength regime with a large number of switchable input or output ports.

3.3. In-Line Filter Results

The square lattice EBG in-line filter configuration is shown in Fig. 10. In this figure the shaded regions are again GaAs (the waveguides and the EBG background substrate) and the black regions are the locations of the metallic rods. The EBG structure consisted of 11 columns × 31 rows, the center column being removed and replaced by the slab waveguide. The distance between the centers and the radii of the metal posts were, as indicated in Fig. 2b, $a = 16$ and $r = 6$, respectively. This in-line filter was tested with the broad bandwidth 3-cycle input pulse. The resulting spectra of the input waveguide pulse, the reflected waveguide pulse and the waveguide pulse transmitted through the filter are shown in Fig. 11. They have been normalized by the peak of the power spectrum of the input waveguide pulse. The stopband is centered at $1.20f_0 = 120\,\text{GHz}$. The full bandwidth of the filter is $6.0\,\text{GHz}$ or 5.0%, which is quite broad. This in-line filter was then driven with the narrow bandwidth excitation at $1.20f_0$. The measured time histories were appropriately truncated to account for the time of arrivals of the fields at the reflected and transmitted field collection ports. It was found that the total reflected power was 94.03% of the input power; the total power output from the device was 1.75% of the input power. This corresponds to a $S_{11} = -0.53\,\text{dB}$ and $S_{12} = -35.15\,\text{dB}$. The remaining power mainly remained within the field structure of the device; i.e., to achieve the filtering response, the appropriate field interference effects must ramp up within the EBG structure. Once the driving pulse leaves the EBG structure, the
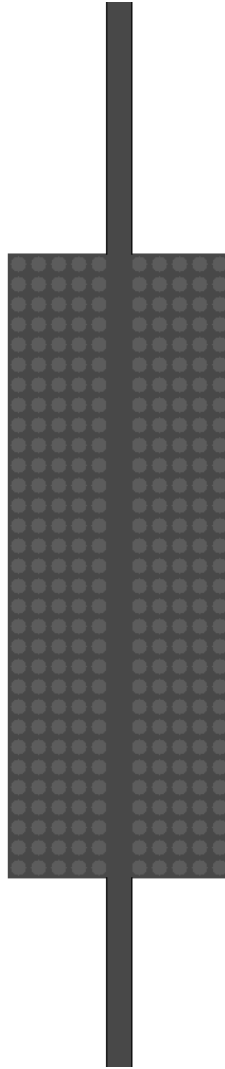
Figure 10. EBG square lattice, circular rod, in-line stopband filter configuration.
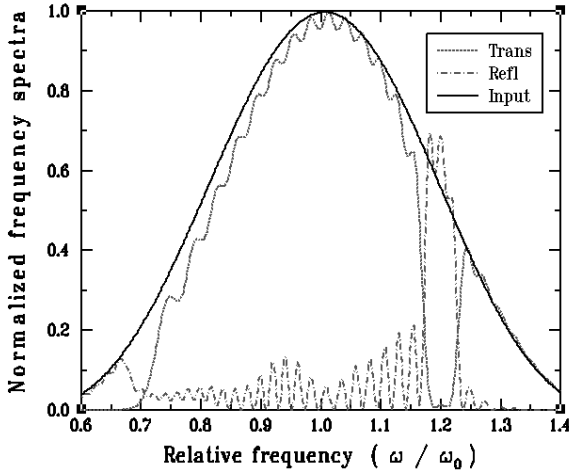
Figure 11. Normalized power spectra results for a broad bandwidth excitation of the EBG square lattice, circular rod, in-line stopband filter.

structure itself rings down and emits power into the input and output waveguides.

It has been shown previously at optical frequencies [9] that maintaining the waveguide size while using thicker rods pushes the center frequency of the stopband to lower values; that air holes rather than metallic rods cause the structure to have a much more complex, less desirable filtering behavior; that more rows will enhance the amount of filtering; that square rods rather than circular rods produce narrower stopbands, but require more rows to achieve similar levels of filtering; and that composite filters to achieve multiple stopbands can be constructed by cascading the appropriate EBG structures immediately one after the other with no gaps in between them. As expected, the same behaviors were obtained in this millimeter-wave regime.

4. CONCLUSIONS

A variety of results were presented that demonstrate the effectiveness of metallo-dielectric EBG structures in the millimeter-wave regime. A Y-power splitter was demonstrated that utilized a triangular EBG structure. A reconfigurable switch concept was demonstrated that utilized the introduction of a current filament to produce the same effects as a metallic post to block the flow of electromagnetic power

into one arm of the Y-power splitter. A completely reconfigurable EBG structure could be achieved with this concept. An integrated millimeter-wave stopband filter was demonstrated. Throughout, the FDTD simulation approach proved to be a very effective and versatile method to model these complex combinations of materials and structures.

Even more complicated EBG configurations can be modeled with the FDTD approach. More complex materials and structures are readily included. This flexibility of the FDTD simulator makes it a very useful design tool for use in EBG device investigations, whether they are studied in the microwave, millimeter or optical wave regimes.

ACKNOWLEDGMENT

REFERENCES

1. Joannopoulos, J. D., R. D. Meade, and J. N. Winn, *Photonics Crystals: Molding the Flow of Light*, Princeton University Press, Princeton, NJ, 1995.

2. Foresi, J. S., P. R. Villeneuve, J. Ferrera, E. R. Thoen, G. Steinmeyer, S. Fan, J. D. Joannopoulos, L. C. Kimerling, H. I. Smith, and E. P. Ippen, "Photonic-bandgap microcavities in optical waveguides," *Nature*, Vol. 390, No. 6656, November 1997.

3. Painter, O., R. K. Lee, A. Scherer, A. Yariv, J. D. O'Brien, P. D. Dapkus, and I. Kim, "Two-dimensional photonic band-gap defect mode laser," *Science*, Vol. 284, No. 5421, 1819–1821, June 1999.

4. Vuckovic, J., O. Painter, X. Yong, A. Yariv, and A. Scherer, "Finite-difference time-domain calculation of the spontaneous emission coupling factor in optical microcavities," *IEEE J. Quan. Electronics*, Vol. 35, No. 8, 1168–1175, August 1999.

5. Benisty, H., C. Weisbuch, D. Labilloy, M. Rattier, C. J. M. Smith, T. F. Krauss, R. M. de-la-Rue, R. Houdre, U. Oesterle, C. Jouanin, and D. Cassagne, "Optical and confinement properties of two-dimensional photonic crystals," *J. Lightwave Tech.*, Vol. 17, No. 11, 2063–2077, November 1999.

6. Scherer, A., O. Painter, A. Husain, J. Vuckovic, D. Dapkus, and

J. O'Brien, "Photonic crystal nanocavity lasers," *Int. J. High Speed Electr. Sys.*, Vol. 10, No. 1, 387–391, March 2000.

7. Weisbuch, C., H. Benisty, and R. Houdre, "Microcavities, photonic crystals and semiconductors: From basic physics to applications in light emitters," *Int. J. High Speed Electr. Sys.*, Vol. 10, No. 1, 339–354, March 2000.

8. Lee, R. K., O. Painter, B. Kitzke, A. Scherer, and A. Yariv, "Emission properties of a defect cavity in a two-dimensional photonic bandgap crystal slab," *J. Opt. Soc. Am. B*, Vol. 17, No. 4, 629–633, April 2000.

9. Painter, O., A. Husain, A. Scherer, P. T. Lee, I. Kim, J. D. O'Brien, and P. D. Dapkus, "Lithographic tuning of a two-dimensional photonic crystal laser array," *IEEE Photonics Tech. Lett.*, Vol. 12, No. 9, 1126–1128, September 2000.

10. Smith, C. J. M., T. F. Krauss, H. Benisty, M. Rattier, C. Weisbuch, U. Oesterle, and R. Houdre, "Directionally dependent confinement in photonic-crystal microcavities," *J. Opt. Soc. Am. B*, Vol. 17, No. 12, 2043–2051, December 2000.

11. Olivier, S., C. Smith, M. Rattier, H. Benisty, C. Weisbuch, T. Krauss, R. Houdre, and U. Oesterle, "Miniband transmission in a photonic crystal coupled-resonator optical waveguide," *Opt. Lett.*, Vol. 26, No. 13, 1019–1021, July 1, 2001.

12. Sigalas, M. M., R. Biswas, and K. M. Ho, "Theoretical study of dipole antennas on photonic band-gap materials," *Microwave Opt. Tech. Lett.*, Vol. 13, No. 4, 205–209, November 1996.

13. Radisic, V., Y. Qian, R. Coccioli, and T. Itoh, "Novel 2-D photonic bandgap structure for microstrip lines," *IEEE Microwave Guided Wave Lett.*, Vol. 8, No. 2, 69–71, February 1998.

14. Rumsey, I., M. Piket-May, and P. K. Kelly, "Photonic bandgap structures used as filters in microstrip circuits," *IEEE Microwave Guided Wave Lett.*, Vol. 8, No. 10, 336–338, October 1998.

15. Smith, G. S., M. P. Kesler, and J. G. Maloney, "Dipole antennas used with all-dielectric, woodpile photonic-bandgap reflectors: gain, field patterns, and input impedance," *Microwave Opt. Tech. Lett.*, Vol. 21, No. 3, 191–196, May 1999.

16. Sigalas, M. M., R. Biswas, K. M. Ho, W. Leung, G. Tuttle, and D. D. Crouch, "The effect of photonic crystals on dipole antennas," *Electromagnetics*, Vol. 19, No. 3, 291–303, May–June 1999.

17. Fei, R. Y., P. M. Kuang, Q. Yongxi, and T. Itoh, "A uniplanar compact photonic-bandgap (UC-PBG) structure and its

applications for microwave circuit," *IEEE Trans. Microwave Theory Tech.*, Vol. 47, No. 8, 1509–1514, August 1999.

18. Coccioli, R., R. Y. Fei-Ran, P. M. Kuang, and T. Itoh, "Aperture-coupled patch antenna on UC-PBG substrate," *IEEE Trans. Microwave Theory Tech.*, Vol. 47, No. 11, 2123–2130, November 1999.

19. Gonzalo, R., P. De-Maagt, and M. Sorolla, "Enhanced patch-antenna performance by suppressing surface waves using photonic-bandgap substrates," *IEEE Trans. Microwave Theory Tech.*, Vol. 47, No. 11, 2131–2138, November 1999.

20. Thevenot, M., C. Cheype, A. Reineix, and B. Jecko, "Directive photonic-bandgap antennas," *IEEE Trans. Microwave Theory Tech.*, Vol. 47, No. 11, 2115–2122, November 1999.

21. Collardey, S., G. Poilasne, A. C. Tarot, P. Pouliguen, C. Terret, and K. Mahdjoubi, "Metallic photonic bandgap propagation mode characterization," *Microwave Opt. Tech. Lett.*, Vol. 28, No. 6, 434–440, March 2001.

22. Serier, C., C. Cheype, R. Chantalat, M. Thevenot, T. Monediere, A. Reineix, and B. Jecko, "1-D photonic bandgap resonator antenna," *Microwave Opt. Tech. Lett.*, Vol. 29, No. 5, 312–315, June 5, 2001.

23. Sailing, H., M. Popov, M. Qiu, L. Zhigang, and C. Simovski, "Explicit formulas for obtaining the radiation characteristics of an antenna based on a three-dimensional metallic photonic bandgap structure," *Microwave Opt. Tech. Lett.*, Vol. 29, No. 6, 376–381, June 20, 2001.

24. Min, Q. and H. Sailing, "High-directivity patch antenna with both photonic bandgap substrate and photonic bandgap cover," *Microwave Opt. Tech. Lett.*, Vol. 30, No. 1, 41–44, July 2001.

25. Reynolds, A. L., H. M. H. Chong, I. G. Thayne, J. M. Arnold, and P. De-Maagt, "Analysis of membrane support structures for integrated antenna usage on two-dimensional photonic-bandgap structures," *IEEE Trans. Microwave Theory Tech.*, Vol. 49, No. 7, 1254–1261, July 2001.

26. Hill, M. J., R. W. Ziolkowski, and J. Papapolymerou, "Simulated and measured results from a Duroid-based planar MBG cavity resonance filter," *IEEE Microwave and Guided Wave Letters*, Vol. 10, No. 12, 528–530, December 2000.

27. Hill, M. J., R. W. Ziolkowski, and J. Papapolymerou, "A high-Q reconfigurable planar EBG cavity resonator," *IEEE Microwave and Wireless Components Letters*, Vol. 11, No. 6, 255–257, June 2001.

28. McGurn, A. R. and A. A. Maradudin, "Photonic band structures of two- and three-dimensional periodic metal or semiconductor arrays," *Phys. Rev. B*, Vol. 48, 17576–17579, December 1993.

29. Kuzmiak, V., A. A. Maradudin, and F. Pincemin, "Photonic band structures of two-dimensional systems containing metallic components," *Phys. Rev. B*, Vol. 50, No. 23, 16835–16844, December 1994.

30. Sigalas, M. M., C. M. Soukoulis, C. T. Chan, and K. M. Ho, "Electromagnetic-wave propagation through dispersive and absorptive photonic-band-gap materials," *Phys. Rev. B*, Vol. 49, No. 16, 11080–11087, April 1994.

31. Sigalas, M. M., C. T. Chan, K. M. Ho, and C. M. Soukoulis, "Metallic photonic band-gap materials," *Phys. Rev. B*, Vol. 52, No. 16, 11744–11751, October 1995.

32. Sievenpiper, D. F., M. E. Sickmiller, and E. Yablonovitch, "3D wire mesh photonic crystals," *Phys. Rev. Lett.*, Vol. 76, No. 14, 2480–2483, April 1996.

33. Scalora, M., M. J. Bloemer, A. S. Pethel, J. P. Dowling, C. M. Bowden, and A. S. Manka, "Transient, metallo-dielectric, one-dimensional, photonic band-gap structures," *J. Appl. Phys.*, Vol. 83, No. 5, 2377–2383, March 1998.

34. Sievenpiper, D. F., E. Yablonovitch, J. N. Winn, S. Fan, P. R. Villeneuve, and J. D. Joannopoulos, "3D metallo-dielectric photonic crystals with strong capacitive coupling between metallic islands," *Physical-Review-Letters*, Vol. 80, No. 13, 2829–3230, March 1998.

35. Bloemer, J. M. and M. Scalora, "Transmissive properties of Ag/MgF$_2$ photonic band gaps," *Appl. Phys. Lett.*, Vol. 72, No. 14, 1676–1678, April 1998.

36. Contopanagos, H., N. G. Alexopoulos, and E. Yablonovitch, "High-Q radio-frequency structures using one-dimensionally periodic metallic films," *IEEE Trans. Microwave Theory Tech.*, Vol. 46, No. 9, 1310–1312, September 1998.

37. Lie, M. L., Q. Z. Zhao, and Z. Xiangdong, "Transmission and absorption properties of two-dimensional metallic photonic-band-gap materials," *Phys. Rev. B*, Vol. 58, No. 23, 15589–15594, December 1998.

38. Sigalas, M. M., R. Biswas, K. M. Ho, C. M. Soukoulis, D. Turner, B. Vasiliu, S. C. Kothari, and S. Lin, "Waveguide bends in three-dimensional layer-by-layer photonic bandgap materials," *Microwave Opt. Tech. Lett.*, Vol. 23, No. 1, 56–59, October 1999.

39. El-Kady, I., M. M. Sigalas, R. Biswas, K. M. Ho, and C. M. Souk-oulis, "Metallic photonic crystals at optical wavelengths," *Phys. Rev. B*, Vol. 62, No. 23, 15299–15302, December 15, 2000.

40. Taflove, A., *Computational Electrodynamics*, Artech House, Norwood, MA, 1995.

41. Taflove, A., *Advances in Computational Electrodynamics*, Artech House, Norwood, MA, 1998.

42. Ziolkowski, R. W. and M. Tanaka, "Finite-difference time-domain modeling of dispersive material photonic band-gap structures," *J. Opt. Soc. Am. A*, Vol. 16, No. 4, 930–940, April 1999.

43. Hill, M. J., R. W. Ziolkowski, and J. Papapolymerou, "Electronically controlled microwave bandgap filter structures," *Appl. Phys. Lett.*, Vol. 78, February 12, 2001.

44. Maloney, J. G., M. P. Kesler, B. L. Shirley, and G. S. Smith, "A simple description for waveguiding in photonic bandgap materials," *Microwave Opt. Tech. Lett.*, Vol. 14, No. 5, 261–266, April 1997.

45. Kuchinsky, S., D. C. Allan, N. F. Borrelli, and J. C. Cotteverte, "3D localization in a channel waveguide in a photonic crystal with 2D periodicity," *Opt. Comm.*, Vol. 175, No. 1–3, 147–152, February 2000.

46. Adibi, A., R. K. Lee, Y. Xu, A. Yariv, and A. Scherer, "Design of photonic crystal optical waveguides with singlemode propagation in the photonic bandgap," *Electr. Lett.*, Vol. 36, No. 16, 1376–1378, August 2000.

47. Adibi, A., X. Yong, R. K. Lee, A. Yariv, and A. Scherer, "Properties of the slab modes in photonic crystal optical wave-guides," *J. Lightwave Tech.*, Vol. 18, No. 11, 1554–1564, November 2000.

48. Lalanne, Ph. and H. Benisty, "Out-of-plane losses of two-dimensional photonic crystals waveguides: Electromagnetic analysis," *J. Appl. Phys.*, Vol. 89, No. 2, 1512–1514, January 2001.

49. Ctyroky, J., "Photonic bandgap structures in planar waveguides," *J. Opt. Soc. Am. A*, Vol. 18, No. 2, 435–441, Feb. 2001.

50. Smith, C. J., R. M. De-La-Rue, M. Rattier, S. Olivier, H. Benisty, C. Weisbuch, T. F. Krauss, R. Houdre, and U. Oesterle, "Coupled guide and cavity in a two-dimensional photonic crystal," *Appl. Phys. Lett.*, Vol. 78, No. 11, 1487–1489, March 2001.

51. Weisbuch, C., H. Benisty, S. Olivier, M. Rattier, C. J. M. Smith, and T. F. Krauss, "3D control of light in waveguide-based two-dimensional photonic crystals," *IEICE Trans. Comm.*, Vol. E84-

B, No. 5, 1286–1294, May 2001.

52. Adibi, A., X. Yong, R. K. Lee, A. Yariv, and A. Scherer, "Guiding mechanisms in dielectric-core photonic-crystal optical waveguides," *Phys. Rev. B*, Vol. 64, No. 3, 033308/1–4, July 15, 2001.

53. Adibi, A., X. Yong, R. K. Lee, M. Loncar, A. Yariv, and A. Scherer, "Role of distributed Bragg reflection in photonic-crystal optical waveguides," *Phys. Rev. B*, Vol. 64, No. 4, 041102/1–4, July 15, 2001.

54. Ziolkowski, R. W. and M. Tanaka, "FDTD analysis of PBG waveguide power splitters and switches for integrated optics applications," *Integrated Photonics Research*, OSA Technical Digest, 194–196, Optical Society of America, Washington, DC, 1999.

55. Ziolkowski, R. W., and M. Tanaka, "FDTD analysis of PBG waveguides, power splitters, and switches," *Opt. Quan. Electr.*, Vol. 31, 843–855, October 1999.

56. Ziolkowski, R. W., "FDTD modeling of electromagnetic bandgap waveguide structures and devices," *Proceedings of AP2000*, Session 2A1, Davos, Switzerland, April 2000.

57. Ziolkowski, R. W., "Electromagnetic bandgap waveguide filters for microwave and optical applications," *Proceedings of ISAP 2000*, Fukuoka, Japan, August 2000.

58. Palik, E. D., *Handbook of Optical Constants of Solids*, 443, Academic Press, Orlando, FL, 1985.

59. Kong, J. A., *Electromagnetic Wave Theory*, John Wiley & Sons, New York, 1986.

60. Wittwer, D. C. and R. W. Ziolkowski, "Two time-derivative lorentz material (2TDLM) formulation of a maxwellian absorbing layer matched to a lossy medium," *IEEE Trans. Antennas and Propagat.*, Vol. 48, 192–199, February 2000.

61. Wittwer, D. C. and R. W. Ziolkowski, "Maxwellian material based absorbing boundary conditions for lossy media in 3D," *IEEE Trans. Antennas and Propagat.*, Vol. 48, 200–213, February 2000.

62. Wittwer, D. C. and R. W. Ziolkowski, "The effect of dielectric loss in FDTD simulations of microstrip structures," *IEEE Trans. Microwave Theory Tech.*, Vol. 49, February 2001.

63. Hurle, D. T. J., "Material for GaAs integrated circuits," *GaAs Integrated Circuits*, J. Mun (Ed.), BSP Professional Books, Oxford, UK, 1988.